

STM Imaging of Flux Line Arrangements in the Peak Effect Regime

A. M. Troyanovskii,* M. van Hecke, N. Saha, J. Aarts, and P. H. Kes

*Kamerlingh Onnes Laboratory, Universiteit Leiden,
PO Box 9504, 2300 RA Leiden, The Netherlands*

(Dated: March 22, 2022)

We present the results of a study of vortex arrangements in the peak-effect regime of 2H-NbSe₂ by scanning tunneling microscopy. By slowly increasing the temperature in a constant magnetic field, we observed a sharp transition from collective vortex motion to positional fluctuations of individual vortices at the temperature which coincides with the onset of the peak effect in ac-susceptibility. We conclude that the peak effect is a disorder driven transition, with the pinning energy winning from the elastic energy.

PACS numbers: 74.60.Ge, 64.60.Cn

It is well known that the critical current density j_c in weakly disordered type II superconductors shows a sudden increase when the applied magnetic field H approaches the upper critical field H_{c2} [1]. An explanation for this intriguing phenomenon, known as the peak effect, was suggested by Pippard [2] already in 1969. It is based on the competition between the collective work done by the disorder (the pinning centers) on the vortex lattice (VL) and the elastic energy stored in vortex lattice deformations due to the pinning [3]. The work depends linearly on $(H_{c2} - H)$ while the elastic energy essentially is proportional to the shear modulus c_{66} of the VL, which behaves as $(H_{c2} - H)^2$. Therefore, at some field close to H_{c2} , the pinning will exceed the elasticity and the VL will accommodate to the random pinning potential, leading to the sudden increase in j_c observed experimentally. The discovery of the high temperature superconductors made it relevant to also consider thermal fluctuations as a third energy scale, which lead to melting by suppression of c_{66} . This would then yield a peak effect as a precursor of the melting transition [4, 5, 6].

Experimentally, it is hard to probe which mechanism is predominant, because one needs information about structural changes of the vortex lattice positional order as a function of time. Small angle neutron scattering (SANS) yields structural information along the field direction averaged over the sample volume, i.e., about the amount of entanglement of the VL. SANS has been successfully used in the peak-effect regime [7, 8, 9] but it is resolution limited in the transverse direction. Lorentz microscopy [10], scanning Hall probe (SHP) [11], scanning SQUID [12, 13] and, recently, magneto-optics experiments [14] yield positional information on the scale of individual vortices, but sense the magnetic field distribution, and only work in the low flux density regime, usually far below H_{c2} , where vortices are well separated and the vortex-vortex interaction is very weak. In this Letter we show that information on the time-dependent positional order can be provided by scanning tunneling microscopy (STM), which is uniquely able to access the necessary length scales and flux densities. We present

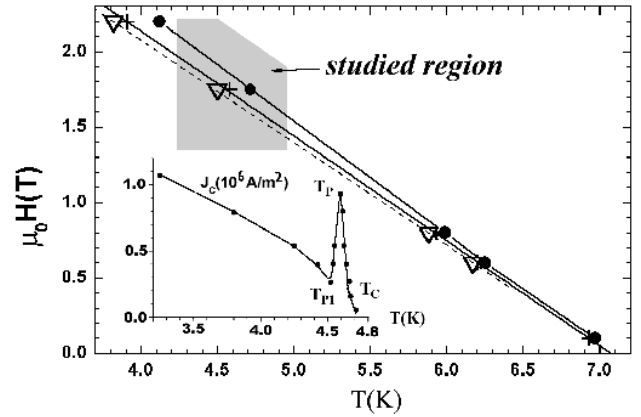


FIG. 1: Phase diagram of NbSe₂ obtained from susceptibility measurements on a single crystal, showing $H_{c2}(T)$ (solid line / circles), the peak of critical current $H_p(T)$ (solid line / plusses) and the onset of the peak $H_{p1}(T)$ (dashed line / triangles). The inset shows the peak effect in the bulk critical current density using the method due to Clem [16, 17] for a flat sample in perpendicular field vs temperature at $\mu_0 H = 1.75$ T.

STM data of vortex structures obtained on a pure single crystal of 2H-NbSe₂ at temperatures around 4.5 K (far below $T_c = 7.1$ K) in the regime of the peak effect. We observed a sharp transition from collective vortex motion to positional fluctuations of individual vortices at a temperature which coincides with the onset of the peak effect in ac-susceptibility measurements. The state above the onset temperature is characterized by the fact that the shear modulus of the VL does not play a role and shows the properties of a pinned liquid.

Fig. 1 shows part of the H, T -phase diagram of one of our crystals as obtained from magnetization measurements with the field along the c -axis (perpendicular to the cleaved surface). Also shown (inset) is the critical current density j_c as function of temperature T in a constant field of 1.75 T, obtained from the maximum of the out-of-phase component of the ac-susceptibility [16, 17]. With this method the same pinning conditions hold for the entire sample and geometrical effects are taken into

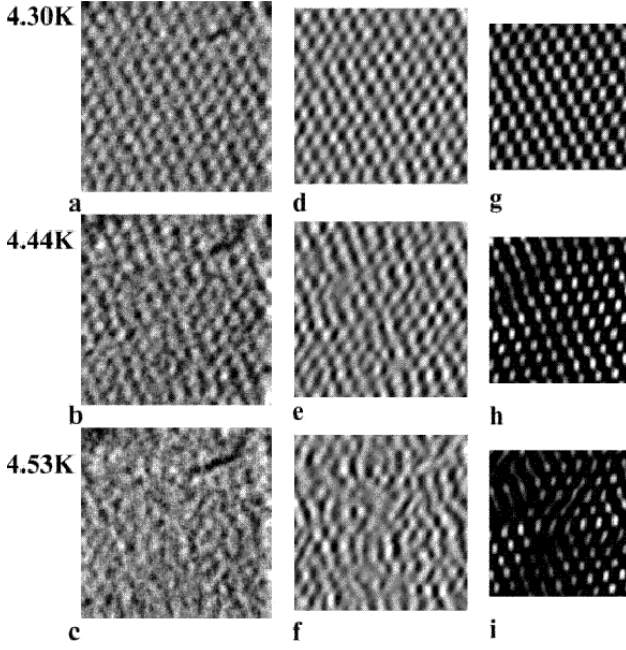


FIG. 2: Raw and processed data from one sequence of STM images acquired at 1.75 T for three different temperatures. The frame size is about 410x460 nm. Left (a-c) : original images (the dark elongated stain in the upper-right corner is caused by a surface defect); middle (d-f) : result of convolution with the shape of "single vortex", right (g-i) : result of convolution with "perfect" lattice cell of 3x3 units.

account. The peak effect sets in at $T_{p1} \simeq 4.5$ K, it reaches a maximum at $T_p \simeq 4.6$ K, and superconductivity disappears at $T_c(H) \simeq 4.7$ K. It should be noticed that in dc-magnetization (SQUID) measurements no peak effect was observed due to flux creep. This means that even in the peak-effect regime nonuniform flux distributions decay within a few minutes to a uniform flux density.

The STM setup was the same as in a previous report [18], with the sample immersed in liquid helium. After decreasing the magnetic field from above H_{c2} at 4.27 K to a preset value (e.g. 1.75 T) in persistent mode (relative decay less than $5 \times 10^{-8} \text{ s}^{-1}$), we waited about 10 minutes before starting the STM imaging. By closing the evaporation valve during imaging a slow temperature rise was established at a rate of $5 \times 10^{-5} \text{ K/s}$ to a value of 4.9 K. The temperature was determined from the pressure with a precision of 2 mK, but we found a small systematic difference between the temperatures of the STM T_{STM} and the SQUID T_{STM} , T_{SQ} , $T_{STM} - T_{SQ} \approx 60 \text{ mK}$, due to the non-uniform temperature in the liquid. We corrected for this difference and estimate the residual uncertainty in the temperature determination to be about 20 mK. The bias voltage was set inside the superconducting gap (0.2-0.8 mV) and the tunnelling current was about 8-15 pA. The signal-to-noise (S/N) ratio goes down when approaching $T_c(H)$, e.g., the relative conductance modu-

lation between vortex core and vortex cell edge decreases from 0.25 (far below T_{p1}) to 0.02 (at T_p). Therefore we had to use a low scanning speed of about 20-70 s per image to acquire images of size 512×512 pixels. The scan area was about 500x500 nm; at a field of 1.75 T we could probe the spatial arrangement of about 150 vortices. The images show a small constant spatial distortion due to a slight asymmetry in the piezo scanner. By heating up in constant field the vortex structure is very weakly perturbed by the almost negligible change of the equilibrium magnetization. The effect of the tunneling current is also expected to be negligible because it is very small ($< 15 \text{ pA}$) and it is directed parallel to the vortices. Moreover, there was no influence on the vortex arrangement when we changed the tunnel current from 7 to 25 pA. In this respect our experiments differ essentially from dc and/or ac-magnetization or transport measurements which do affect the vortex configurations.

Results of experiments at 1.75 T are shown in Fig. 2a-c. We selected three typical temperatures: (a) 4.3 K (well below T_{p1}), (b) 4.44 K (just below T_{p1}) and (c) 4.53 K (between T_{p1} and T_p). The first image shows an almost perfect vortex arrangement without large visible distortions. With increasing temperature we see an increasing shear distortion of the VL and the appearance of VL defects. With a further increase of T the signal from the vortices gradually decreases to the noise level. Several image-processing procedures were used to extract the positional information. The S/N ratio could be considerably improved by convoluting the original data with the images of perfect vortex lattice cells acquired at low T , using cell sizes up to 10x10 vortices. In Figs. 2d-f the results are shown of convolution with 1 vortex ('1x1'), in Figs. 2g-i of convolution with a 3x3 cell, both with respect to the corresponding data in the Figs. 2a-c. Using the 1x1-convolutions, the displacements of individual vortices could be followed up to 4.56 K, see below. The low contrast in Figs. 2e,f is most likely due to noise, but may also denote local vortex displacements.

With the knowledge of the vortex positions, further analysis can be performed using the vortex motion. Inspecting consecutive frames in the temperature interval between 4.3 K and 4.6 K in a field of 1.75 T, we notice a sudden change in the vortex mobility at 4.48 K. Below 4.48 K we find *collective* jumps of large portions of the VL; above 4.48 K, we only see oscillations of individual vortices around fixed positions. An example of a collective jump is given in Fig. 3a, which displays the difference between two consecutive frames of raw data at 4.31 K. The scan direction is horizontal going from bottom to top. In the lower part of the figure the vortex lattice did not move substantially, and the difference gives an impression of the noise level. At the scan position denoted by the arrow the entire VL moved over a considerable fraction of the VL parameter a_0 . The next difference picture (not shown), has a lattice below and noise above

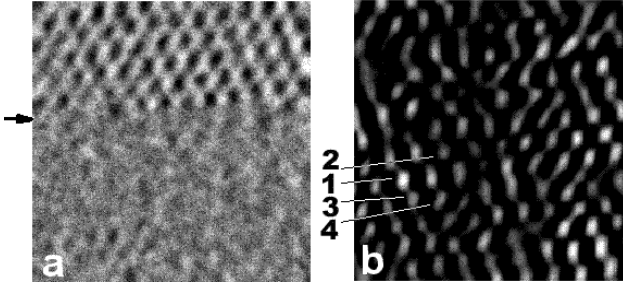


FIG. 3: (a) Difference between two consecutive images at 4.31 K in a field of 1.75 T, to demonstrate coherent motion of vortices. When scanning the second image from bottom to top, the VL moved at the line indicated by the arrow. (b) Average of the sum of 60 consecutive images taken with increasing temperature above T_{p1} . The brightness is a measure for the probability of finding a vortex at a certain position. The numbers indicate individual vortices discussed in the text.

the position of the arrow. We could see no net motion of the VL, it is jumping between metastable positions. Above 4.48 K, no collective jumps were observed; in the 60 images in which T slowly rose to 4.9 K (total observation time about 70 minutes) we did not detect any net motion of individual vortices in the image, although some vortices hopped back and forth between two metastable positions. A movie of the change in behavior, made of 1-cell filtered frames for noise reduction, can be viewed on our website [19].

We can characterize this transition by introducing the following two order parameters, based on the displacement $\vec{d}_{i,n}$ of vortex i going from frame n to frame $n+1$, $\vec{d}_{i,n} = \vec{r}_{i,n+1} - \vec{r}_{i,n}$; (i) δ_n ; in order to quantify the amount of motion of the vortices, we define

$$\delta_n := \left(\frac{1}{N} \sum_i \vec{d}_{i,n}^2 \right)^{1/2} / (a_0), \quad (1)$$

where the sum runs over the N displacement vectors. (ii) K_n ; in order to quantify the amount of *correlated* motion of the vortices, we define

$$K_n := \frac{1}{N} \sum_{\langle i,k \rangle} \frac{\vec{d}_{i,n} \cdot \vec{d}_{k,n}}{|\vec{d}_{i,n}| \cdot |\vec{d}_{k,n}|}, \quad (2)$$

where the sum runs over the displacements on neighboring vortices i and k in a range $1.5 a_0$. For both parameters, only contributions were retained for which $\vec{d}_{i,n}$ was two or more pixels.

Clearly, when vortices move coherently, both δ_n and K_n will be large, while for uncorrelated, random motion, K_n is small but δ_n remains finite. Both K_n and δ_n are plotted versus T in Fig. 4a,b. For both, the behavior abruptly changes at $T_{STM} = 4.48$ K, which is essentially T_{p1} (see Fig. 1). Below T_{p1} the behavior of K_n exhibits the collective vortex lattice jumps between metastable positions in the collective pinning potential. At T_{p1} , the

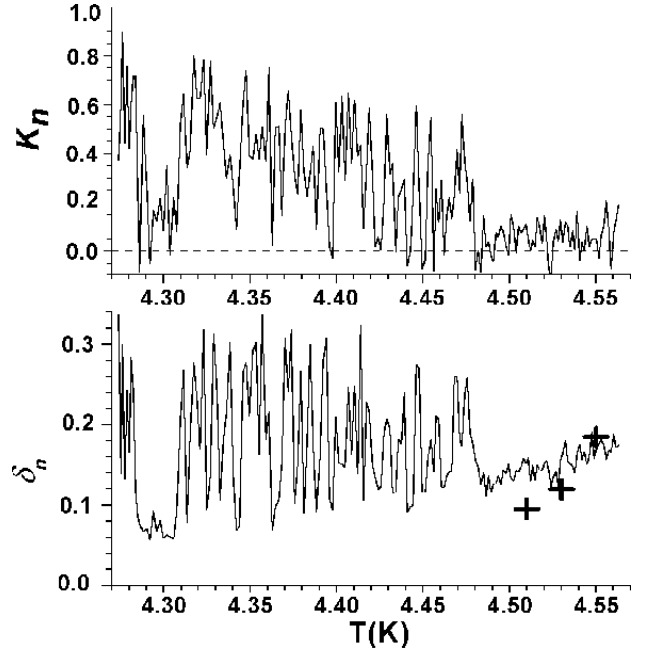


FIG. 4: (a) Order parameter K_n for the correlated displacement of vortices from frame to frame as function of temperature at a magnetic field of 1.75 T. (b) Amplitude of vortex displacement δ_n averaged over the total number of vortices in a frame in the same sequences of images. Symbols (+) mark the value $\sqrt{2} \langle u^2 \rangle / a_0$ (the value of δ_n for fluctuations of individual vortices) calculated from the average of 4 selected vortices (see Fig. 3 and Table 1).

picture suddenly changes to a situation in which each vortex independently fluctuates within its own pin potential. The sudden drop of K_n to the noise level reflects this transition from collective to single vortex behavior. From the plot of δ_n versus T it follows that the collective jumps span a distance of about 0.1 - 0.25 a_0 , which changes at T_{p1} to individual jumps with a much smaller amplitude spread. The distance of collective jumps reflects the typical length scale separating independent local minima in the pinning potential in the field regime close to H_{c2} (at low fields where the vortex cores are well separated, this scale would be the Ginzburg-Landau coherence length ξ). The jumps occur more frequently with increasing temperature.

From the original STM pictures it can be also concluded that the jumps are directed along the principal axes of the VL. In the regime above T_{p1} the mean-squared displacement gradually grows with temperature to a value $\langle u^2 \rangle^{1/2} \sim 0.1 a_0$. This number is close to the Lindemann criterion for melting, $\langle u^2 \rangle^{1/2} = c_L a_0$ with $c_L \sim 0.15 - 0.25$. However, we do not observe diffusive motion of vortices over more than a_0 . This is illustrated in Fig. 3b where 60 images in the temperature regime above T_{p1} are averaged. Since the noise level for all vortices is supposedly the same, the brightness of the spots represent the probability amplitude for finding a vortex

at a certain position. The brightest spots display vortices with an almost fixed position. One of them is marked #1; other vortices (marked #2–4) are less bright, indicating larger individual positional oscillations most likely caused by thermal fluctuations.

TABLE I: Mean square displacement $\langle u^2 \rangle^{1/2} / a_0$ at three temperatures between T_{p1} and T_p for the four vortices indicated in Fig. 3b.

Vortex number:	#1	#2	#3	#4
4.51 K	0.045	0.095	0.055	0.077
4.53 K	0.055	0.080	0.13	0.071
4.55 K	0.070	0.10	0.21	0.15

In Table 1 the values are given of $\langle u^2 \rangle^{1/2} / a_0$ for these 4 vortices determined from 20 images around the denoted temperatures. Near the onset of the peak effect (4.51 K) the amplitudes remain far below the Lindemann criterion. Approaching T_p , the amplitudes for the vortices #3 and #4 increase to values close to the Lindemann criterion. However, the estimated average of $\langle u^2 \rangle^{1/2} / a_0$ for all detectable vortices coincides with the data in Fig. 4b and remains well below the criterion for melting. Therefore, and because of the absence of large scale vortex diffusion within the 70 minutes observation time, we have shown that the change at T_{p1} signifies a disorder driven transition from collective pinning to single vortex pinning. The consequence is a sudden change in the temperature and/or field dependence of the critical current which causes the peak effect.

Following this main result we add a few quantitative remarks about the observed disorder and the relation of our result to those in other papers. From the convoluted images we can extract some information about the size of the Larkin domains in the temperature range below the peak effect (although the limited number of vortices in the images does not allow much statistics). The positional order in an area of 10x10 vortices disappears at a T_{STM} of about 4.35 K, while for an area of 6x6 vortices positional order is seen up to T_{p1} . The computed correlation lengths from the Fourier transform of the images have similar values: $(4 - 6)a_0$ at the onset of the peak effect and $\sim (1 - 2)a_0$ above the onset temperature. It should be noted this the correlation length is about twice as large as the transverse size of the Larkin domain R_c . At the onset of the peak effect the value of R_c/a_0 drops from about 3 to 1. This result is in reasonable agreement with the values we obtained in a previous analysis of critical current data on a similar crystal [17]. Based on SANS experiments on a Nb single crystal, Ling *et al.* [8] found evidence for supercooling and superheating of the vortex matter disorder around the peak effect line in the phase diagram and concluded that this is direct structural evidence for a first-order vortex solid-liquid transition. Very

recent SANS work of Forgan *et al.* [9] demonstrated that the vortex solid in very pure Nb is stable to very close to the $H_{c2}(T)$ line. This shows that the history dependence observed by Ling *et al.* is disorder driven rather than of thermal origin and this is in agreement with the disorder driven transition seen in our STM experiment.

In conclusion, the mechanism for the peak effect is the conquest of the pinning energy over the elastic energy, just as was first suggested by Pippard [2], and later in more detail described by Larkin and Ovchinnikov [20]. The high temperature phase is characterized by the fact that the shear energy has become irrelevant. In this phase, the vortices are not free to move around as one would expect to occur in a liquid, but they remain trapped in their own pin potential which may differ for each vortex. In terms of the collective pinning theory this would be the amorphous limit, but it would be equally correct to say that we are dealing with a pinned liquid.

This work is part of the research program of the "Stichting FOM", which is financially supported by NWO. It was partially supported by the Dutch-Russian science collaboration financed by NWO, and by the ESF network 'Vortex'. We thank R. Drost for assistance in the early experiments.

* Permanent Address : Institute for High Pressure Physics, Russian Academy of Science, Troitsk, 142092, Russia.

- [1] M. A. R. Le Blanc and W. A. Little, in *Proceeding of the VII International Conference on Low Temperature Physics 1960* (University of Toronto Press, Toronto), p.198, 1960.
- [2] A. B. Pippard, *Philos. Mag.* **19**, 217 (1969).
- [3] G. Blatter *et al.*, *Rev. Mod. Phys.* **66**, 1125 (1994).
- [4] P. Berghuis and P.H. Kes, *Phys. Rev. B* **47**, 262 (1993).
- [5] S. Bhattacharya and M.J. Higgins, *Physica C* **257**, 232 (1996).
- [6] X.S. Ling, J.E. Berger and D.E. Prober, *Phys. Rev. B* **57**, R3249 (1998).
- [7] P.L. Gammel *et al.*, *Phys. Rev. Lett.* **80**, 833 (1998).
- [8] X. S. Ling *et al.*, *Phys. Rev. Lett.* **86**, 712 (2001).
- [9] E.M. Forgan *et al.*, *Phys. Rev. Lett.* **88**, 167003 (2002).
- [10] A. Tonomura *et al.*, *Nature*, **412**, 620 (2001).
- [11] A. Oral *et al.*, *Phys. Rev. Lett.* **80**, 3610 (1998).
- [12] B. L. T. Plourde *et al.*, *Physica C* **341**, 1023 (2000).
- [13] J. R. Kirtley *et al.*, *Phys. Rev. Lett.* **76**, 1336 (1996).
- [14] P. E. Goa *et al.*, *Supercond. Sci. Technol.* **14**, 729 (2001).
- [15] M. Marchevsky, M. J. Higgins and S. Bhattacharya, *Nature*, **409** 591 (2001).
- [16] J. R. Clem and A. Sanchez, *Phys. Rev. B* **50**, 9355 (1994).
- [17] L.A. Angurel *et al.*, *Phys. Rev. B* **56**, 3425 (1997).
- [18] A.M. Troyanovski, J.Aarts, P.H.Kes, *Nature*, **399**, 665 (1999).
- [19] <http://www.physics.leidenuniv.nl/sections/cm/msm>
- [20] Larkin A. I. and Ovchinnikov Yu. N., *J. Low Temp. Phys.* **34**, 409 (1979).